(tsh, August-September-October 2005)

Polarization correlations and the Bell states: Single-mode and multi-mode treatments

These notes look at the polarization correlation of the Bell states and related analogues of those states. Coincidence probabilities of single-mode and multi-mode states are calculated as a function of the polarization analyzer angles and plotted for different experimental situations.

Single-mode analyses

The four Bell states are

$$\left|\Psi^{(\pm)}\right\rangle = \frac{1}{\sqrt{2}}\left(\left|H\right\rangle_1\left|V\right\rangle_2 \pm \left|V\right\rangle_1\left|H\right\rangle_2\right) \tag{1}$$

$$\left|\Phi^{(\pm)}\right\rangle = \frac{1}{\sqrt{2}}\left(\left|H\right\rangle_1\left|H\right\rangle_2 \pm \left|V\right\rangle_1\left|V\right\rangle_2\right), \tag{2}$$

where

$$\left|H\right\rangle_j = h_j^\dagger\left|\text{vac}\right\rangle \quad \text{and} \quad \left|V\right\rangle_j = v_j^\dagger\left|\text{vac}\right\rangle \qquad \left(j = 1,2\right) \tag{3}$$

are single-modes representing photons propagating in the jth direction and having horizontal and vertical polarizations, respectively. Together, the four Bell states form a complete set for the joint Hilbert space of the two particle system. The entangled nature of the Bell states leads to several interesting physical properties, including non-local correlations, which can be detected experimentally. Here we consider polarization correlation experiments using the Bell states defined above, as well as more arbitrary analogues of these states.

When a polarizer is placed into either path 1 or 2, the creation operator of the output mode is defined as

$$a_j^\dagger = h_j^\dagger \cos\theta_j + v_j^\dagger \sin\theta_j, \tag{4}$$

for $j = 1,2$, where θ_j is the angle of the linear polarizer's transmission axis with respect to the axis of horizontal polarization. The commutation relations

$$\left[a_j, h_k^\dagger\right] = \cos\theta_j \delta_{jk} \tag{5}$$

$$\left[a_j, v_k^\dagger\right] = \sin\theta_j \delta_{jk} \tag{6}$$

also relate the input and output modes. The probability for an output mode to be populated after passage of a Bell state through a titled linear polarizer is given by

$$P_j^{\Psi\pm}(\theta_j) = \left\langle \Psi^{(\pm)} \middle| a_j^\dagger a_j \middle| \Psi^{(\pm)} \right\rangle = \frac{1}{2} \tag{7}$$

$$P_j^{\Phi\pm}(\theta_j) = \left\langle \Phi^{(\pm)} \middle| a_j^\dagger a_j \middle| \Phi^{(\pm)} \right\rangle = \frac{1}{2}. \tag{8}$$

So, for any of the four Bell states there is a 50:50 chance that a photon will pass through the analyzer present in output mode j, independent of the angle at which the polarizer is set.

For comparison, the one-photon state

$$|\psi\rangle = \cos\theta |H\rangle_1 + \sin\theta |V\rangle_1 \tag{9}$$

has a probability to pass through a polarizer given by

$$\langle\psi| a_1^\dagger a_1 |\psi\rangle = \cos^2(\theta_1 - \theta), \tag{10}$$

which is unity when the polarizer angle matches the mixing angle θ. We also consider an ensemble of the single-photon states given by Eq. (9), where each member differs in the value of θ. For a uniform distribution $f(\theta) = (2\pi)^{-1}$ of initial states, the probability to pass through the polarizer is given by

$$\int_0^{2\pi} d\theta f(\theta) \left| a_1 |\psi\rangle \right|^2 = \frac{1}{2\pi} \int_0^{2\pi} d\theta \cos^2(\theta_1 - \theta) = \frac{1}{2}. \tag{11}$$

Returning to the Bell states, the probabilities for joint detection of a photon in modes 1 and 2 are

$$P^{\Psi\pm}(\theta_1, \theta_2) = \left\langle \Psi^{(\pm)} \middle| a_1^\dagger a_2^\dagger a_2 a_1 \middle| \Psi^{(\pm)} \right\rangle = \frac{1}{2} \sin^2(\theta_1 \pm \theta_2) \tag{12}$$

$$P^{\Phi\pm}(\theta_1, \theta_2) = \left\langle \Phi^{(\pm)} \middle| a_1^\dagger a_2^\dagger a_2 a_1 \middle| \Phi^{(\pm)} \right\rangle = \frac{1}{2} \cos^2(\theta_1 \mp \theta_2). \tag{13}$$

This calculation is a straightforward application of the commutation rules in Eqs. (5) and (6). The joint probabilities in Eqs. (12) and (13) are not products of the individual probabilities, as would be the case for a factorizable two-photon state. The conditional probabilities,

$$P_c^{\Psi\pm}(\theta_2 \mid \theta_1) = P^{\Psi\pm}(\theta_1, \theta_2) / P_1^{\Psi\pm}(\theta_1) = \sin^2(\theta_1 \pm \theta_2) \tag{14}$$

$$P_c^{\Phi\pm}(\theta_2 \mid \theta_1) = P^{\Phi\pm}(\theta_1, \theta_2) / P_1^{\Phi\pm}(\theta_1) = \cos^2(\theta_1 \mp \theta_2), \tag{15}$$

demonstrate that the likelihood of a photon passing through the polarizer in mode 2 depends on the value of the polarizer setting in mode 1. For example, when $\theta_1 = \theta_2$, the

conditional probability of Eq. (14) yields zero while for $\theta_2 = \theta_1 + \pi/2$ the same probability is unity. Together these results imply that the photons in modes 1 and 2 are always orthogonally polarized, which agrees with the form of Eq. (1). However, the polarizers may be arbitrarily far apart and the polarizer angles set independently, even after the state has been prepared. Therefore the outcome of one measurement seemingly influences a distant, independently-chosen measurement. This non-local correlation is the essence of polarization-entangled photons; despite being spatially separated, polarization measurements remain correlated. Similar arguments follow from Eq. (15) to indicate that both photons in the state $\left|\Phi^{\pm}\right\rangle$ have parallel polarizations, c.f. Eq. (2).

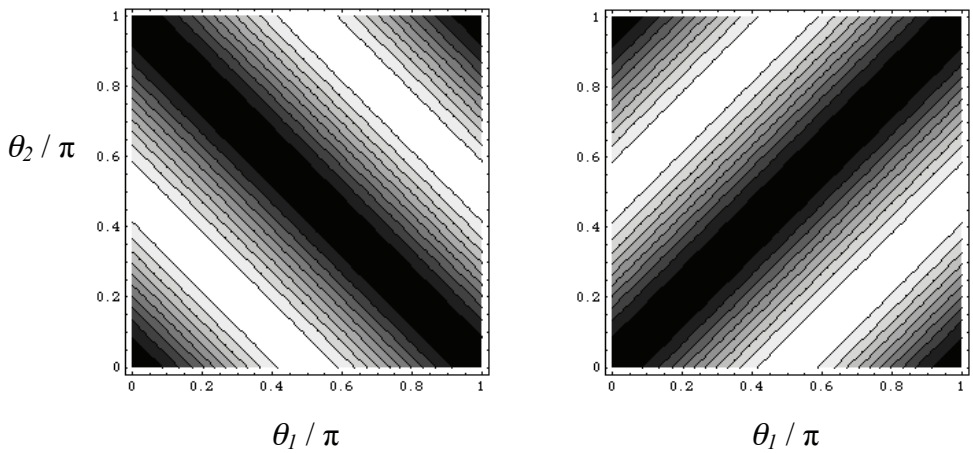

Fig. 1. The conditional probabilities (left) $P^{\Psi+}(\theta_2 \mid \theta_1)$ and (right) $P^{\Psi-}(\theta_2 \mid \theta_1)$. Angles are measured in units of π and lighter shading indicates higher probability density, as measured by the equally spaced contours.

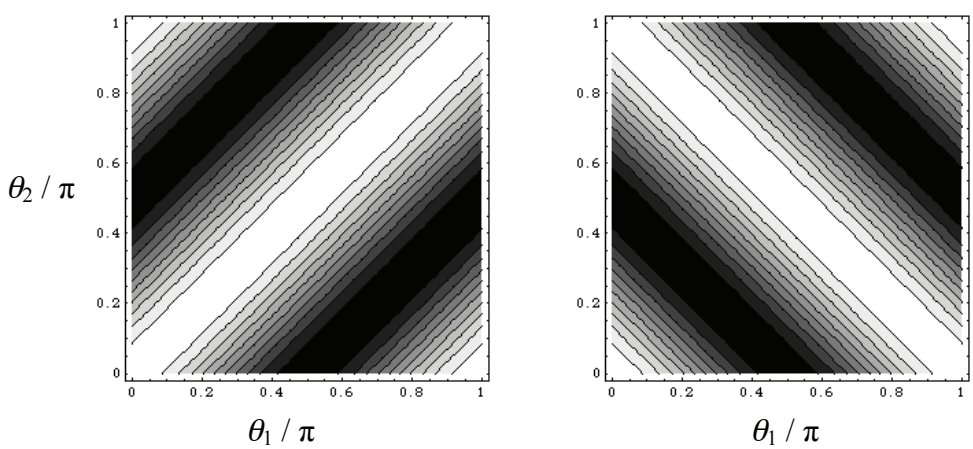

Fig. 2. The conditional probabilities (left) $P^{\Phi+}(\theta_2 \mid \theta_1)$ and (right) $P^{\Phi-}(\theta_2 \mid \theta_1)$. Angles are measured in units of π and lighter shading indicates higher probability density, as measured by the equally spaced contours.

We also consider the entangled states

$$\left|\Psi(\alpha)\right\rangle = \frac{1}{\sqrt{2}}\left(\left|H\right\rangle_1\left|V\right\rangle_2 + e^{i\alpha}\left|V\right\rangle_1\left|H\right\rangle_2\right) \tag{16}$$

$$\left|\Phi(\alpha)\right\rangle = \frac{1}{\sqrt{2}}\left(\left|H\right\rangle_1\left|H\right\rangle_2 + e^{i\alpha}\left|V\right\rangle_1\left|V\right\rangle_2\right), \tag{17}$$

where α is a real constant phase. Kwiat et al. [Phys. Rev. Lett. **75**, 4337 (1995)] , as well as others, have used a similar expression in their analysis of polarization-entangled photon pairs generated from spontaneous parametric down conversion. In those experiments, the relative phase α arises from the crystal birefringence and nonzero transit times for the oppositely-polarized photons. Kwiat et al. point out that an additional birefringent phase shifter can be placed in mode 1 (or 2?) to set the value of α as desired. [Is it possible to characterize the action of the phase α as a rotation on a Poincaré sphere for the two-photon state? Does such a representation, analogous to the single-photon state, exist?] Note that the von Neumann/Shannon entropy of these states is maximal, just as with the original Bell states.

From our prior definitions of the Bell states in Eqs. (1) and (2), we rewrite

$$\left|\Psi(\alpha)\right\rangle = e^{i\alpha/2}\left[\cos(\alpha/2)\left|\Psi^+\right\rangle - i\sin(\alpha/2)\left|\Psi^-\right\rangle\right] \tag{18}$$

$$\left|\Phi(\alpha)\right\rangle = e^{i\alpha/2}\left[\cos(\alpha/2)\left|\Phi^+\right\rangle - i\sin(\alpha/2)\left|\Phi^-\right\rangle\right], \tag{19}$$

from which we obtain the original Bell states by selecting the appropriate values of α :

$$\left|\Psi^+\right\rangle = \left|\Psi(0)\right\rangle \text{ and } \left|\Psi^-\right\rangle = \left|\Psi(\pi)\right\rangle \tag{20}$$

$$\left|\Phi^+\right\rangle = \left|\Phi(0)\right\rangle \text{ and } \left|\Phi^-\right\rangle = \left|\Phi(\pi)\right\rangle. \tag{21}$$

The probability of coincidence detection for the state (16) is

$$\begin{aligned} P^{\Psi\alpha}(\theta_1,\theta_2) &= \left|\cos\theta_1\sin\theta_2 + e^{i\alpha}\cos\theta_2\sin\theta_1\right|^2 \\ &= \cos^2(\alpha/2)\sin^2(\theta_1+\theta_2) + \sin^2(\alpha/2)\sin^2(\theta_1-\theta_2), \end{aligned} \tag{22}$$

which is the weighted sum of the probabilities for the two orthogonal Bell-state components, c.f. (12). This classical average results from complete cancellation of the interference terms, i.e.

$$\left\langle\Psi^-\left|a_1^\dagger a_2^\dagger a_2 a_1\right|\Psi^+\right\rangle = \left\langle\Psi^+\left|a_1^\dagger a_2^\dagger a_2 a_1\right|\Psi^-\right\rangle \tag{23}$$

regardless of the polarizer settings or the value of α. We similarly calculate the coincidence count of state (17) to be

$$P^{\Phi\alpha}(\theta_1,\theta_2) = \left|\cos\theta_1\cos\theta_2 + e^{i\alpha}\sin\theta_2\sin\theta_1\right|^2 \tag{24}$$
$$= \cos^2(\alpha/2)\cos^2(\theta_1-\theta_2) + \sin^2(\alpha/2)\cos^2(\theta_1+\theta_2),$$

and again find the result to be a weighted superposition of the result for the corresponding Bell states, c.f. Eq. (13).

Choosing specific values of α, Eqs. (22) and (24) yield the conditional probabilities for coincidence detection of the quasi-Bell states. This result is highlighted in the contour plots of Fig. 3, where $\alpha = 0.5\pi$ and the coincidence probabilities are equally weighted sums; the left and right fringe patterns in Fig. 3 could also be obtained by averaging the left and right panels of Figs. 1 and 2, respectively.

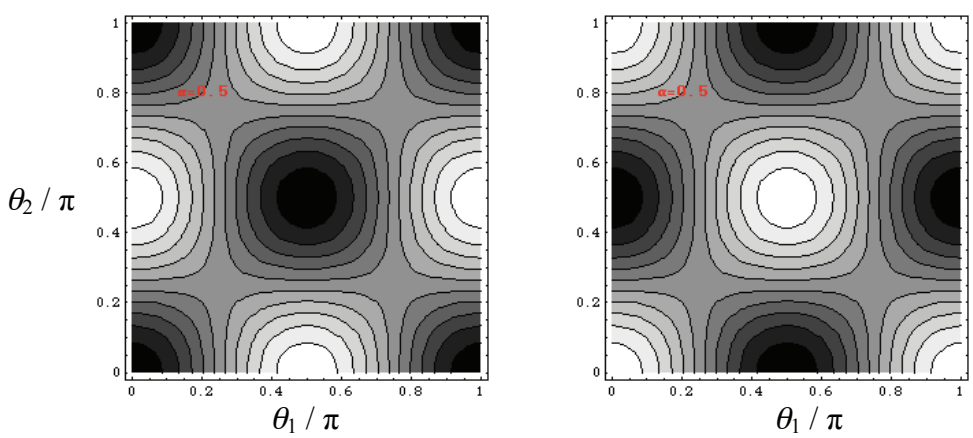

Fig. 3. The conditional probabilities (left) $P_c^{\alpha}(\theta_2 \mid \theta_1)$ and (right) $P_c^{\prime\alpha}(\theta_2 \mid \theta_1)$ for the case of $\alpha = 0.5\pi$. Angles are measured in units of π and lighter shading indicates higher probability density, as quantified by the equally spaced contours.

It is instructive to consider another form of entangled state,

$$\left|\vartheta(\beta)\right\rangle = \frac{1}{\sqrt{2}}\left(\left|L\right\rangle_1\left|V\right\rangle_2 + e^{i\beta}\left|R\right\rangle_1\left|H\right\rangle_2\right), \tag{25}$$

where the left- and right-handed states of circular polarization are defined as

$$\left|L\right\rangle_1 = \frac{1}{\sqrt{2}}\left(\left|H\right\rangle_1 + i\left|V\right\rangle_1\right) \text{ and } \left|R\right\rangle_1 = \frac{1}{\sqrt{2}}\left(\left|H\right\rangle_1 - i\left|V\right\rangle_1\right), \tag{26}$$

respectively. The state (25) could be obtained, for instance, by generating the entangled state defined by Eq. (16) and then inserting a quarter-wave plate into the path of mode 1. When the quarter-wave plate is oriented at 45° with respect to the horizontal-polarization axis, its action on the photon in mode 1 may be represented in matrix notation as

$$Q \doteq \frac{1}{\sqrt{2}}\begin{pmatrix} 1 & i \\ i & 1 \end{pmatrix}, \tag{27}$$

with the subsequent effects that

$$Q|H\rangle_1 \doteq \frac{1}{\sqrt{2}}\begin{pmatrix} 1 & i \\ i & 1 \end{pmatrix}\begin{pmatrix} 1 \\ 0 \end{pmatrix} \doteq |L\rangle_1 \text{ and } Q|V\rangle_1 \doteq \frac{1}{\sqrt{2}}\begin{pmatrix} 1 & i \\ i & 1 \end{pmatrix}\begin{pmatrix} 1 \\ 0 \end{pmatrix} \doteq i|R\rangle_1. \tag{28}$$

In the case the state given by Eq. (16) is the input to a quarter-wave plate, the resulting phase will be $\beta = \alpha - \pi/2$.

We may also write the entangled state defined by Eq. (25) as

$$|\vartheta(\beta)\rangle = \frac{1}{\sqrt{2}}\left(|\Psi^-(\beta + \pi/2)\rangle + i|\Phi^-(\beta + \pi/2)\rangle\right). \tag{29}$$

For the case the $\beta = \pi/2$ we prepare the state

$$|\vartheta(\beta = \pi/2)\rangle = \frac{1}{\sqrt{2}}\left(|\Psi^+\rangle + i|\Phi^+\rangle\right), \tag{30}$$

while for $\beta = -\pi/2$ we have

$$|\vartheta(\beta = -\pi/2)\rangle = \frac{1}{\sqrt{2}}\left(|\Psi^-\rangle + i|\Phi^-\rangle\right). \tag{31}$$

Now we consider the probability to detect a photon in mode 1 of $|\vartheta(\beta)\rangle$. For the entangled state given by Eq. (25),

$$P^{\vartheta\beta}(\theta_1) = \langle\vartheta(\beta)|a_1^\dagger a_1|\vartheta(\beta)\rangle = \frac{1}{2}. \tag{32}$$

This is the same detection probability found for a single circularly-polarized mode which passes through a polarizer, i.e.

$$\langle L|a^\dagger a|L\rangle = \langle R|a^\dagger a|R\rangle = \frac{1}{2}. \tag{33}$$

The probability of coincidence detection for the entangled two-photon state is

$$P^{\vartheta\beta}(\theta_1,\theta_2) = \langle\vartheta(\beta)|a_1^\dagger a_2^\dagger a_2 a_1|\vartheta(\beta)\rangle = \frac{1}{4}\left(1 + \sin(2\theta_2)\cos(2\theta_1 - \beta)\right), \tag{34}$$

The conditional probability for joint detection is

$$P^{\vartheta\beta}(\theta_2 \mid \theta_1) = \frac{1}{2}\left(1 + \sin(2\theta_2)\cos(2\theta_1 - \beta)\right). \tag{35}$$

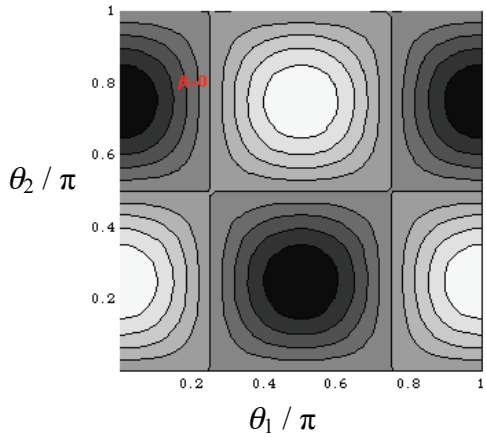

Fig. 4. The joint probability for detection of the state (25) with $\beta = 0$. Angles are measured in units of π and lighter shading indicates higher probability, as quantified by the equally spaced contours.

Multimode analyses

Expressions (1) and (2) for the Bell states can be extended to incorporate multimode states, i.e. photonic wave packets of finite temporal and nonzero spectral widths. These states more accurately describe the polarization-entangled photon pairs generated by recent experiments using spontaneous parametric down conversion (SPDC). Multimode character is especially relevant when the pump pulse is of an ultrashort duration. Then, the sub-picosecond coherence time of the pump pulse shortens the temporal window during which the signal and idler photons can be generated, as compared to the (in principle) infinite time window for pair generation in the case of a cw pump.

Multimode analogs of Eq. (1) and (2) are formulated as

$$\left|\tilde{\Psi}^{(\pm)}\right\rangle = \frac{1}{\sqrt{2}}\int_0^\infty d\omega \int_0^\infty d\omega' \left[f(\omega,\omega')h_1^\dagger(\omega)v_2^\dagger(\omega') \pm g(\omega,\omega')v_1^\dagger(\omega)h_2^\dagger(\omega')\right]\left|\text{vac}\right\rangle, \tag{36}$$

$$\left|\tilde{\Phi}^{(\pm)}\right\rangle = \frac{1}{\sqrt{2}}\int_0^\infty d\omega \int_0^\infty d\omega' \left[f(\omega,\omega')h_1^\dagger(\omega)h_2^\dagger(\omega') \pm g(\omega,\omega')v_1^\dagger(\omega)v_2^\dagger(\omega')\right]\left|\text{vac}\right\rangle, \tag{37}$$

where $f(\omega,\omega')$ and $g(\omega,\omega')$ are scalar functions determined by the properties of the pump field, the $\chi^{(2)}$ medium governing the SPDC process, and the placement of the detectors. Normalization of Eqs. (36) and (37) requires

$$\int_0^\infty d\omega \int_0^\infty d\omega \left|f(\omega,\omega')\right|^2 + \int_0^\infty d\omega \int_0^\infty d\omega \left|g(\omega,\omega')\right|^2 = 2, \tag{38}$$

[N.B. In general the functions f and g are different for the anti-symmetric $\left(\tilde{\Psi}\right)$ and symmetric $\left(\tilde{\Phi}\right)$ states, and are dependent on the type of SPDC process, either type-I or type-II; we use the same symbols for the two-photon amplitudes in Eqs. (36) and (37) merely as a convenience. Note however that there are experimental means by which the symmetric and anti-symmetric states can be converted between each other without significantly altering the two-photon amplitude. See for example P. G. Kwiat et al., Phys. Rev. A **60**, R773 (1999), where half-wave plates are used to rotate polarization components.]

The frequency-dependent modes of the analyzer are

$$a_j(\omega) = h_j(\omega)\cos\theta_j + v_j(\omega)\sin\theta_j \qquad j = 1,2, \tag{39}$$

where the creation operators satisfy the commutation relations

$$\left[h_j(\omega), h_k^\dagger(\omega')\right] = 2\pi\delta(\omega-\omega')\delta_{jk} \qquad \text{and} \qquad \left[v_j(\omega), v_j^\dagger(\omega')\right] = 2\pi\delta(\omega-\omega')\delta_{jk}.$$

Our assumption that the transmission angles of the polarizers are independent of frequency may only be valid when the bandwidth of the incident light is sufficiently narrow. [What are the practical limits of this assumption? Does a breakdown of the approximation manifest in experiments?] Extensions of the commutation relations given by Eqs. (5) and (6) follow.

From the multi-mode Bell states, we calculate the detection probability behind each polarizer as:

$$P_j^{\tilde{\Psi}\pm}(\theta_j) = \int_0^\infty d\overline{\omega} \left\langle \tilde{\Psi}^{(\pm)} \middle| a_j^\dagger(\overline{\omega}) a_j(\overline{\omega}) \middle| \tilde{\Psi}^{(\pm)} \right\rangle \tag{40}$$

$$= \frac{1}{2}\int_0^\infty d\overline{\omega} \int_0^\infty d\overline{\omega}' \left(\left|f(\overline{\omega},\overline{\omega}')\right|^2 \cos^2\theta_j + \left|g(\overline{\omega},\overline{\omega}')\right|^2 \sin^2\theta_j \right)$$

$$P_j^{\tilde{\Phi}\pm}(\theta_j) = \int_0^\infty d\overline{\omega} \left\langle \tilde{\Phi}^{(\pm)} \middle| a_j^\dagger(\overline{\omega}) a_j(\overline{\omega}) \middle| \tilde{\Phi}^{(\pm)} \right\rangle \tag{41}$$

$$= \frac{1}{2}\int_0^\infty d\overline{\omega} \int_0^\infty d\overline{\omega}' \left(\left|f(\overline{\omega},\overline{\omega}')\right|^2 \cos^2\theta_j + \left|g(\overline{\omega},\overline{\omega}')\right|^2 \sin^2\theta_j \right)$$

For the case that

$$\int_0^\infty d\omega \int_0^\infty d\omega \left| f(\omega,\omega') \right|^2 = \int_0^\infty d\omega \int_0^\infty d\omega \left| g(\omega,\omega') \right|^2 = 1, \tag{42}$$

we find that the conditional probabilities of Eqs. (7) and (8) for detection of a single-photon, as calculated for the single-mode, Bell states, also hold in the multimode case, i.e. they are constant. The corresponding joint probabilities for detection are

$$P^{\Psi\pm}(\theta_1,\theta_2) = \int d\overline{\omega} \int d\overline{\omega}' \left\langle \tilde{\Psi}^{(\pm)} \middle| a_1^\dagger(\overline{\omega}) a_2^\dagger(\overline{\omega}') a_2(\overline{\omega}') a_1(\overline{\omega}') \middle| \tilde{\Psi}^{(\pm)} \right\rangle \tag{43}$$

$$= \frac{1}{2} \int d\overline{\omega} \int d\overline{\omega}' \left| f(\overline{\omega},\overline{\omega}') \cos\theta_1 \sin\theta_2 \pm g(\overline{\omega},\overline{\omega}') \cos\theta_2 \sin\theta_1 \right|^2$$

$$P^{\tilde{\Phi}\pm}(\theta_1,\theta_2) = \int_0^\infty d\overline{\omega} \int_0^\infty d\overline{\omega}' \left\langle \tilde{\Phi}^{(\pm)} \middle| a_1^\dagger(\overline{\omega}) a_2^\dagger(\overline{\omega}') a_2(\overline{\omega}') a_1(\overline{\omega}') \middle| \tilde{\Phi}^{(\pm)} \right\rangle \tag{44}$$

$$= \frac{1}{2} \int_0^\infty d\overline{\omega} \int_0^\infty d\overline{\omega}' \left| f(\overline{\omega},\overline{\omega}') \cos\theta_1 \cos\theta_2 \pm g(\overline{\omega},\overline{\omega}') \sin\theta_2 \sin\theta_1 \right|^2$$

Now it is when

$$\mathrm{Re} \int d\omega \int d\omega' f(\omega,\omega')^* g(\omega,\omega') = 1, \tag{45}$$

or equivalently,

$$f(\omega,\omega') = g(\omega,\omega'), \tag{46}$$

that maximum visibility in the polarization correlation will be observed. As then Eqs. (43) and (44) reduce to the corresponding probabilities found in the single-mode analysis, c.f. Eqs. (12) and (13).

The coincident probability of Eq. (43) agrees with the results of U'Ren et al. [arxiv_quantph_03051192_ABUren.pdf], c.f. their Eq. (13). Their analysis continues by addressing whether type-I and type-II SPDC generated photon pairs can meet the conditions necessary for maximal interference in both a polarization correlation experiment and a HOM/Bell-state interferometer. They assert that the experiment by Paul Kwiat, Edo Waks, and others [P. G. Kiwat et al. Phys. Rev. A **60**, 773 (1999)], which used two type-I SPDC crystals, generated polarization-entangled photons with

sufficiently symmetrized coefficients that the necessary conditions could be meet. We'll consider these points in more detail later, in the Bell-state analyzer notes.

The requirement given by Eq. (45) for maximal visibility in the polarization correlation emphasizes the role played by the multimode nature of the entangled-photons. Unlike the familiar, maximally-entangled Bell states, the multimode superposition states in Eqs. (36) and (37) are not generally composed of two indistinguishable outcomes. Rather, the amplitudes $f(\omega,\omega')$ and $g(\omega,\omega')$ determine the spectral and temporal properties of the two possible polarizations, *H-V* and *V-H*, respectively. (In the single-mode Bell states, both amplitudes are equated with unity). Consequently, one may be able to distinguish between the two possible down-conversion outcomes though the observation of their spectral and temporal properties.

The effects of distinguishing information are important in the use of entangled photons prepared by type-II spontaneous parametric down-conversion (SPDC). In SPDC, an incident pump photon is down converted into a pair of photons. The subsequent, lower energy photons, termed the signal and idler, arise from the nonlinear interaction driven by the pump pulse in a $\chi^{(2)}$ birefringent crystal. In the case of type-II SPDC, the signal and idler photons have opposite polarizations and, at certain experimental geometries, are prepared in the anti-symmetric triplet state given by Eq. (36), i.e. $\left|\tilde{\Psi}^{(+)}\right\rangle$. When the incident pump beam is quasi-continuous, the bi-photon spectral amplitude reduces to a delta function and a subsequent analysis using the usual Bell states is applicable. However, the needs of quantum information processing require production of these states on demand, a feat naturally accomplished through the use of a broad-bandwidth, ultrashort-duration pump pulse. A drawback to this approach is that the spectral (and temporal) properties of the signal and idler photons may correlate with their different polarizations.

In type-II SPDC, one finds the two-photon amplitudes given as [W. P. Grice and I. A. Walmsley, Phys. Rev. A **56**, 1627 (1997)]

$$f(\omega,\omega') = \alpha(\omega+\omega')\phi(\omega,\omega') \tag{47}$$

and

$$g(\omega,\omega') = f(\omega',\omega), \tag{48}$$

where $\alpha(\omega)$ is the spectral amplitude of the pump pulse and $\phi(\omega,\omega')$ is the phase-matching function. If we consider the generation of the entangled photon-pair to be collinear with the pump field and to arise from a crystal of finite thickness L and infinite cross section, then the type-II phase-matching function is

$$\phi(\omega,\omega') = N\,\mathrm{sinc}\left[L\left(k_p(\omega+\omega') - k_s(\omega) - k_i(\omega')\right)/2\right] \tag{49}$$
$$\times\exp\left\{-iL\left(k_p(\omega+\omega') - k_s(\omega) - k_i(\omega')\right)/2\right\},$$

where N is a normalization constant specified below and k_μ is the wave vector of the μth field. We approximate the wave vectors of the pump, signal, and idler fields to first-order as

$$k_{s,i}(\omega) \cong k_{s,i}(\omega_0) + (\omega-\omega_0)k'_{s,i}(\omega_0) \tag{50}$$

and

$$k_p(\omega) \cong k_p(2\omega_0) + (\omega-2\omega_0)k'_p(2\omega_0), \tag{51}$$

where $2\omega_0$ is the center frequency of the pump spectrum. Though higher-order terms in these expansion may contribute to the experimentally observed signal [Can they be handled analytically?], we consider only the first-order effects brought on by dispersion. Assuming perfect phase-matching at zeroth order, i.e.

$$k_p(2\omega_0) = k_s(\omega_0) + k_i(\omega_0), \tag{52}$$

the phase-matching function reduces to

$$\phi(\omega,\omega') = N\,\mathrm{sinc}\left[a(\omega-\omega_0) + b(\omega'-\omega_0)\right]e^{-i\left(a(\omega-\omega_0)+b(\omega'-\omega_0)\right)}. \tag{53}$$

where

$$a = L\left(k'_p - k'_s\right)/2 \text{ and } b = L\left(k'_p - k'_i\right)/2 \tag{54}$$

are time constants that characterize the difference between the transit times of the pump and the μth beam through half of a crystal length. For future use we denote

$$\tau_a = 2a, \qquad \tau_b = 2b, \qquad \text{and} \qquad \tau_0 = 2(b-a), \tag{55}$$

where, without loss of generality, we consider $b > a > 0$. [N. B. In general, a and b are determined by the birefringent properties of the crystal, *and* the frequency which we expand about, i.e. the pump center frequency.]

From the second line of Eq. (53), it is apparent that $\phi(\omega,\omega') \neq \phi(\omega',\omega)$ and hence

$$f(\omega,\omega') \neq g(\omega,\omega');$$

the condition for maximal visibility is unfulfilled. The distinction between the amplitudes traces back to the crystal birefringence and the different group velocities of the signal and idler photons in the crystal medium; i.e. $a \neq b$. It is possible to compensate for the different propagation times the signal and idler experience by inserting another birefringent material into the beam path, oriented and cut so that the faster polarization component is slowed down while the slower polarization component propagates freely (or more quickly). However this approach to compensating for phase differences between pathways does not mitigate differences in the absolute value of phase-matching functions. One approach for achieving the latter is to introduce spectral filters in the paths of the two beams. This however trims bandwidth from the photons, lengthens their temporal duration and lowers the overall quantum yield of the entanglement generation process.

To illustrate the dependence of a polarization correlation experiment's visibility on the form of the two-photon amplitude we consider the pump spectrum as a normalized Gaussian centered about $2\omega_0$ with a bandwidth characterized by σ, i.e.

$$\alpha(\omega+\omega') = \left(\pi\sigma^2\right)^{-1/4} \exp\left[-\left(\omega+\omega'-2\overline{\omega}\right)^2/2\sigma^2\right]. \tag{56}$$

Normalization of the two-photon state leads to the phase-matching function as

$$\phi(\omega,\omega') = \left(\frac{b-a}{\pi}\right)^{1/2} \operatorname{sinc}\left[a(\omega-\omega_0)+b(\omega'-\omega_0)\right] e^{-i\left(a(\omega-\omega_0)+b(\omega'-\omega_0)\right)}, \tag{57}$$

c.f. Eq. (53). Calculating the coincident detection probability given by Eqs. (43) and (44) leads to the interference term of interest:

$$I = \int d\omega \int d\omega' f(\omega,\omega')^* g(\omega,\omega') e^{i(\omega\delta_1-\omega'\delta_2)}, \tag{58}$$

where δ_j is the delay acquired by the state after placing a birefringent plate in path *j*. IN many experimental situations these two delay may be equal.

Using Eqs. (47), (48), (53), and (56), the interference integral is expressed as

$$I = \left(\pi\sigma^2\right)^{-1/2}\left(\frac{b-a}{\pi}\right)\int d\omega \int d\omega'\, e^{-(\omega+\omega'-2\omega_0)^2/\sigma^2+i(a-b)(\omega-\omega')+i(\delta_1\omega-\delta_2\omega')} \tag{59}$$

$$\times \operatorname{sinc}\left[a(\omega-\omega_0)+b(\omega'-\omega_0)\right] \operatorname{sinc}\left[a(\omega'-\omega_0)+b(\omega-\omega_0)\right].$$

Evaluation of this integral (see the accompaning Appendix) yields,

$$I = \frac{e^{i\omega_0(\delta_1-\delta_2)}\sqrt{\pi}}{\sigma(\tau_a+\tau_b)}\left\{\left(\mathrm{erf}\left(\frac{\sigma(\delta_1\tau_b+\delta_2\tau_a)}{2\tau_0}\right)+\mathrm{erf}\left(\frac{\sigma(\delta_1\tau_a+\delta_2\tau_b)}{2\tau_0}\right)\right)\Pi(\delta_1+\delta_2;0,\tau_0)\right. \tag{60}$$

$$+\left(\mathrm{erf}\left(\frac{\sigma((\tau_0-\delta_1)\tau_b+(\tau_0-\delta_2)\tau_a)}{2\tau_0}\right)\right.$$

$$\left.\left.+\,\mathrm{erf}\left(\frac{\sigma((\tau_0-\delta_1)\tau_a+(\tau_0-\delta_2)\tau_b)}{2\tau_0}\right)\right)\Pi(\delta_1+\delta_2;\tau_0,2\tau_0)\right\},$$

with $\mathrm{erf}(x)$ the error function and $\Pi(\delta;t_1,t_2)$ the rectangle window function. For the case $\delta_1=\delta_2=\delta$, we have

$$I = \frac{2\sqrt{\pi}}{\sigma(\tau_a+\tau_b)}\left\{\mathrm{erf}\left(\frac{\sigma(\tau_a+\tau_b)\delta}{2\tau_0}\right)\Pi\left(\delta;0,\frac{\tau_0}{2}\right)\right. \tag{61}$$

$$\left.+\mathrm{erf}\left(\frac{\sigma(\tau_a+\tau_b)(\tau_0-\delta)}{2\tau_0}\right)\Pi\left(\delta;\frac{\tau_0}{2},\tau_0\right)\right\}$$

[N.B. Apart from notational differences, this results agrees with Eq. (3.16) in Warren's thesis. There is an overall sign difference because I am using the triplet state, whereas Warren uses the singlet state. In the argument of the error function we substitute $\sigma\to\sigma/\sqrt{2}$ to obtain Warren's result. (One of these days I'll walk the path *more* traveled.)]

As an example of the effect the non-identical photon amplitudes have on the visibility of the polarization correlation experiment, let's consider the pump pulse to be centered at 405 nm with a bandwidth of 0.8 nm, i.e. $\omega_0 = 2.3255\times10^{15}$ rad$\cdot$Hz and $\sigma = 5.51744\times10^{12}$ Hz. Take the nonlinear medium to be a BBO crystal with a length $L = 2$ mm. Using the Sellmeier constants for BBO, [The Handbook of Nonlinear Optical Crystals, page 99], we calculate the indices of refraction for the ordinary and extraordinary polarizations. The collinear phase-matching angle (the angle of the pump and e-ray w.r.t. the crystal axis) is found numerically to be 41.793089 degrees. Again, using the Sellmeier equation, we find the group velocities of the o- and e-rays at ω_0 to be 178.04 ps/µm and 184.261 ps/µm (the e-ray is "faster"). The group velocity of the pump pulse at its center frequency is 175.645 ps/µm. The first-order phase-matching

coefficients defined in Eq. (54) are therefore $a = 76.5969$ fs and $b = 266.239$ fs. Below we show magnitude plots of *f* and *g* and their overlap.

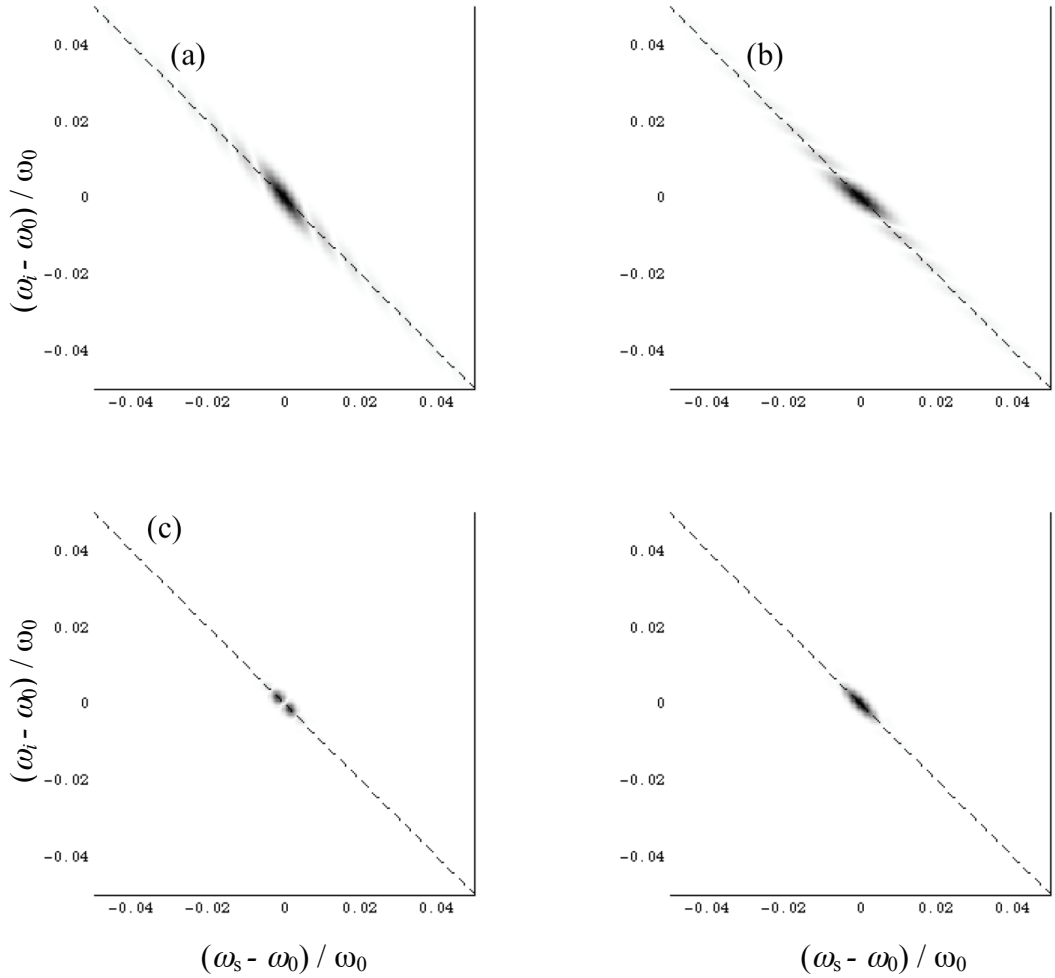

Fig. 5 For a 0.8 nm bandwidth pump pulse: the magnitudes of the two-photon amplitudes *f* and *g* plotted in panels (a) and (b), respectively, as a function of the difference frequency (relative to the degenerate frequency ω_0). In (c) and (d), the real part of the overlap of *f* and *g* are similarly plotted. In (c) no timing correction has been introduced, i.e. $\delta = 0$, while in (d) the interference has been maximized by using $\delta = \tau_0/2$. In all plots, darker regions indicate larger probability amplitude. The dashed line traces the anti-diagonal.

Unlike the magnitude of the interference plotted in Fig. 5(c), the phase of the interference between *f* and *g* can be adjusted by passing the beams through another birefringent crystal, whose axes are oriented so as to compensate for the different group

velocities the o- and e-rays experience in the crystal. The prepared interference, as a function of the added delay, is calculated according to Eq. (61) and shown in Fig. 6.

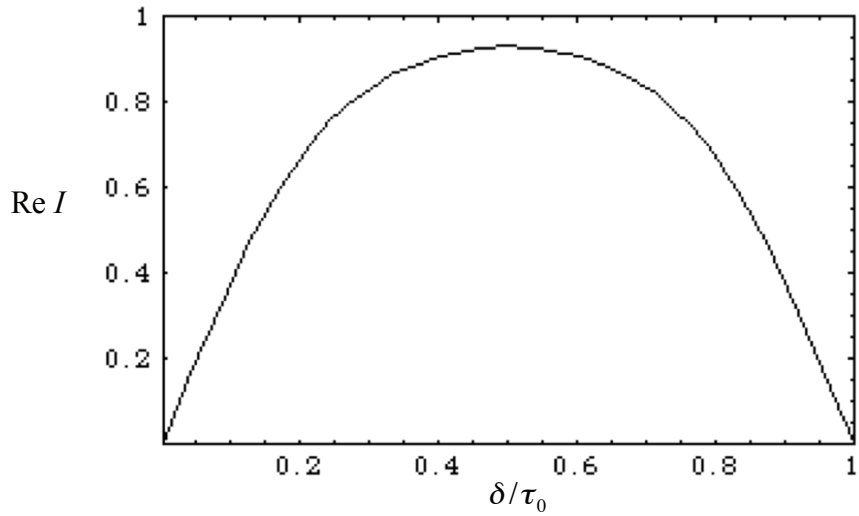

Fig. 6. The interference I as a function of the additional delay δ for a pump pulse with 0.8 nm bandwidth. The delay time is measured in units of $\tau_0 = 379.284$ fs.

Maximal interference occurs when $\delta = \tau_0/2$. Yet the interference is not complete, as demonstrated by a value less than one. The polarization correlation for this scenario, shown in Fig. 7, is different from that of the single mode case presented earlier in Fig. 1.

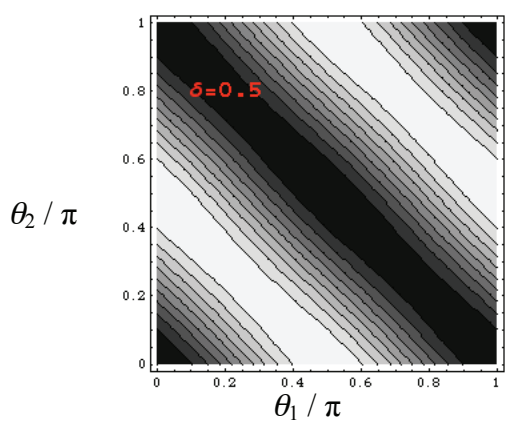

Fig. 7 Polarization correlation for $\left|\tilde{\Psi}^{+}\right\rangle$ in the first scenario. The timing of the photons has been adjusted by introducing an external delay δ, measured in units of τ_0, to the fast component. Angles are measured in units of π and lighter shading indicates higher probability density, as measured by the equally spaced contours

The slight differences between the multimode calculation of the polarization correlation shown in Fig. 7, and the corresponding single mode calculation shown on the

left of Fig. 1, become more noticeable as the bandwidth of the pump pulse increases. We now consider a similar scenario but with a slightly larger pulse bandwidth of 3 nm ($\sigma = 2.06904 \times 10^{13}$ Hz) and calculate the polarization correlation shown in Fig. 8.

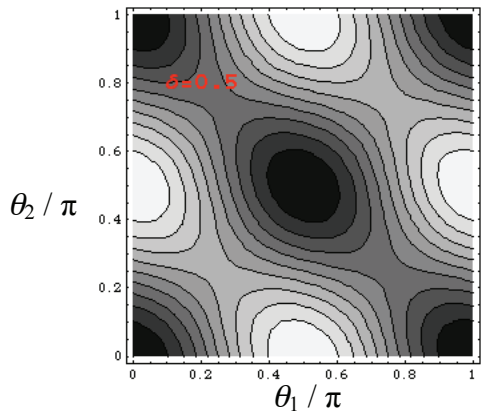

Fig. 8 Polarization correlation for $\left|\tilde{\Psi}^{+}\right\rangle$ in the second scenario. The timing of the photons has been adjusted by introducing an external delay δ, measured in units of τ_0, to the fast component. Angles are measured in units of π and lighter shading indicates higher probability density, as measured by the equally spaced contours

The interference effect is much less prnounced in the case of the larger bandwidth pump pulse, as seen in Fig. 9.

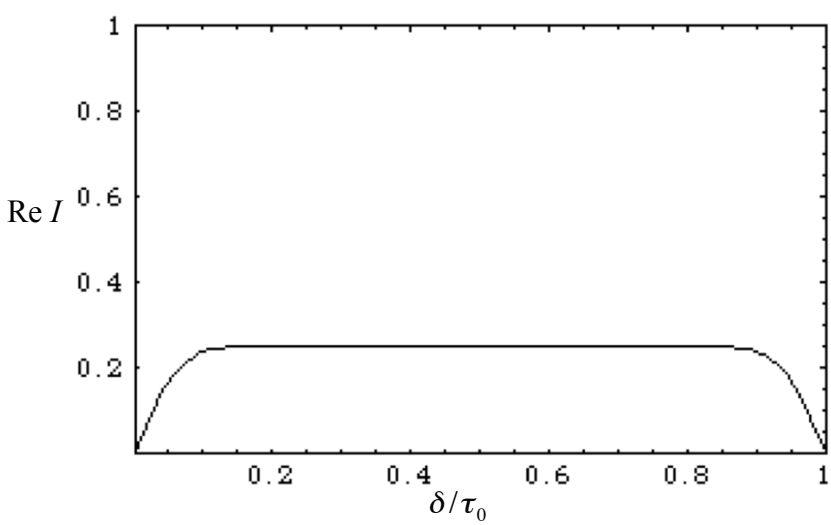

Fig. 9. The interference I as a function of the additional delay δ for a pump pulse with 3.0 nm bandwidth. The delay time is measured in units of $\tau_0 = 379.284$ fs.

For further comparison, note that the two-photon amplitude in the second scenario, shown in Fig. 10, is broader, as compared to Fig. 6. This is due to the greater bandwidth

in the second scenario. However, a reduction in the interference between the two amplitudes results from a greater amount of distinguishing information; *f* and *g* are more dissimilar in the second scenario.

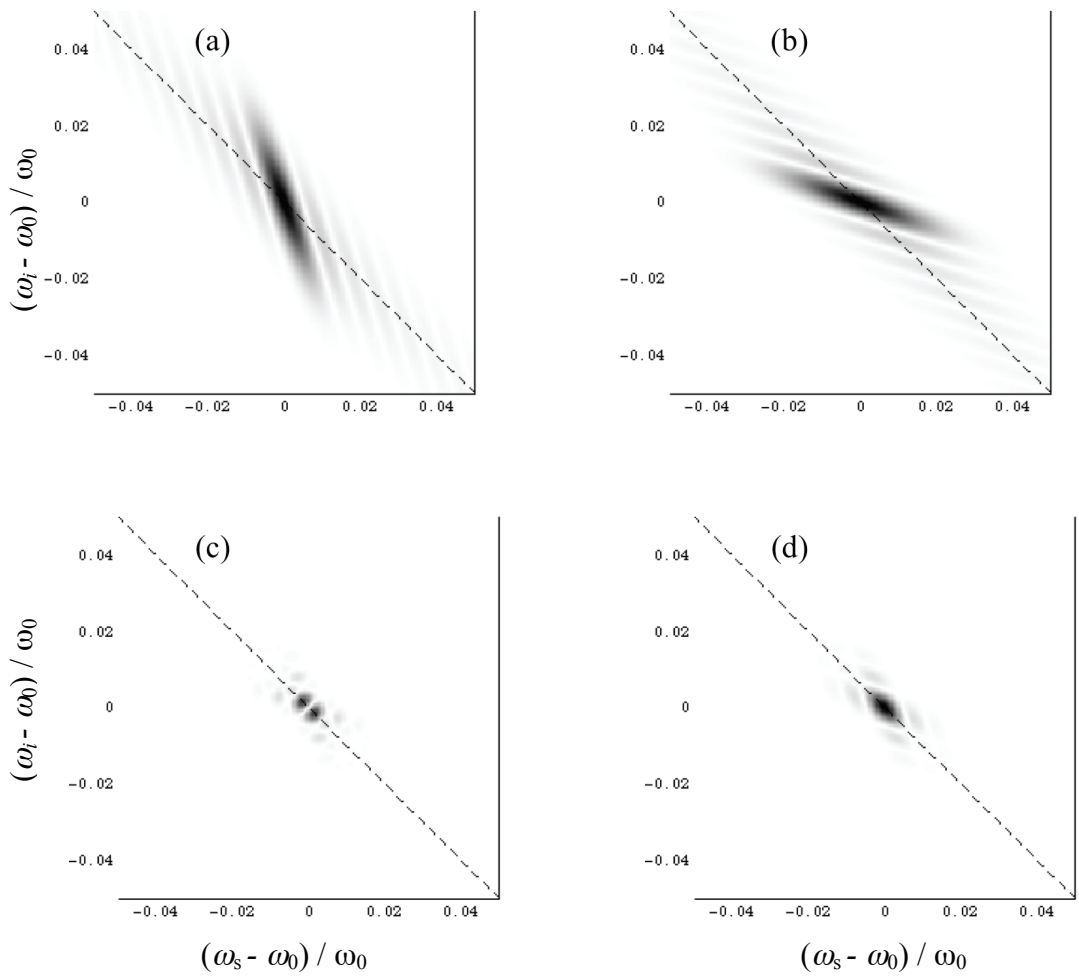

Fig. 10. For a 3.0 nm bandwidth pump pulse: the magnitudes of the two-photon amplitudes *f* and *g* plotted in panels (a) and (b), respectively, as a function of the difference frequency (relative to the degenerate frequency ω_0). In (c) and (d), the real part of the overlap of *f* and *g* are similarly plotted. In (c) no timing correction has been introduced, i.e. $\delta = 0$, while in (d) the interference has been maximized by using $\delta = \tau_0 / 2$. In all plots, darker regions indicate larger probability amplitude. The dashed line traces the anti-diagonal.

Appendix

We define the integral

$$A = \int d\nu \int d\nu' e^{-(\nu+\nu')^2/\sigma^2 + i(a-b)(\nu-\nu') + i(\delta_1\nu - \delta_2\nu)} \tag{A.1}$$
$$\times \operatorname{sinc}[a\nu + b\nu'] \operatorname{sinc}[a\nu' + b\nu],$$

where $\nu = \omega - \omega_0$ and $\nu' = \omega' - \omega_0$ are difference frequencies and

$$I = e^{i\omega_0(\delta_1 - \delta_2)} \left(\pi\sigma^2\right)^{-1/2} \left(\frac{b-a}{\pi}\right) A. \tag{A.2}$$

We have extended the lower limits of integration in A to $-\infty$, under the assumption that the pump bandwidth is much less than the center frequency (Something akin to the rotating wave approximation.) We switch to the sum and difference coordinates

$$x = \nu + \nu' \text{ and } y = \nu - \nu', \tag{A.3}$$

which have the differential area element

$$dxdy = -2d\nu d\nu'. \tag{A.4}$$

In terms of these new coordinates,

$$A = -\frac{1}{2} \int dx e^{-x^2/\sigma^2 + i\Delta x} \int dy e^{i(2\beta + \Sigma)y} \operatorname{sinc}(\alpha x + \beta y) \operatorname{sinc}(\alpha x - \beta y), \tag{A.5}$$

where we have defined the constants

$$\alpha = (a+b)/2 \text{ and } \beta = (a-b)/2 \tag{A.6}$$
$$\Delta = (\delta_1 - \delta_2)/2 \text{ and } \Sigma = (\delta_1 + \delta_2)/2.$$

We make the change of variable

$$y' = \beta y + \alpha x, \tag{A.7}$$

after which A is expressed as

$$A = -\frac{1}{2\beta} \int dx e^{-x^2/\sigma^2 - i\Delta x - i(2+\Sigma')\alpha x} \int dy' e^{i(2+\Sigma')y'} \operatorname{sinc}(y') \operatorname{sinc}(y' - 2\alpha x) \tag{A.8}$$

with $\Sigma' = \Sigma/\beta$ for notational convenience.

Evaluation of the integral over y' can be carried out by using the definition of the sinc function as the inverse Fourier transform of the rectangle function, i.e.

$$\operatorname{sinc}(y) = \frac{\sin y}{y} = \frac{1}{2} \int dz\, e^{-izy} \Pi(z; -1, 1), \tag{A.9}$$

where the rectangle window function is defined as

$$\Pi(z;z_1,z_2)=\begin{cases}1, & z_1\le z\le z_2\\ 0, & \text{otherwise}\end{cases}\quad . \tag{A.10}$$

We consider the integral

$$J(\xi)=\int dy\, e^{i\xi y}\operatorname{sinc}(y)\operatorname{sinc}(y-\Xi). \tag{A.11}$$

which can be rewritten using Eq. as

$$J(\xi)=\frac{\pi}{2}\int dz e^{i(\xi-z)\Xi}\operatorname{rect}(z)\operatorname{rect}(z-\Xi), \tag{A.12}$$

There are two cases of ξ which give non-zero values for $J(\xi)$:

$$J(\xi)=\frac{\pi}{2}e^{i\xi\Xi}\int_{-1+\xi}^{1}e^{-iz\Xi}=\frac{\pi e^{i\xi\Xi/2}}{\Xi}\sin\left[(1-\xi/2)\Xi\right],\qquad 0\le\xi<2, \tag{A.13}$$

and

$$J(\xi)=\frac{\pi}{2}e^{i\xi\Xi}\int_{-1}^{1+\xi}e^{-iz\Xi}=\frac{\pi e^{i\xi\Xi/2}}{\Xi}\sin\left[(1-|\xi|/2)\Xi\right],\qquad -2<\xi\le 0; \tag{A.14}$$

otherwise the integral is zero. This can be reduced to the result

$$J(\xi)=\frac{\pi e^{i\xi\Xi/2}}{\Xi}\sin\left[(1-|\xi|/2)\Xi\right],\qquad |\xi|<2. \tag{A.15}$$

Equating $\xi=2+\Sigma'$ and $\Xi=2\alpha x$, we find

$$A=\frac{\pi}{4(b^2-a^2)}\int dx\frac{e^{-x^2/\sigma^2+i\Delta x}}{x}\sin\left[(2-|2+\Sigma'|)\alpha x\right],\qquad |2+\Sigma'|<2 \tag{A.16}$$

The constraint on Σ' stipulates that to view interference effects, we must have

$$-4<\Sigma'<0\ \Rightarrow\ 0<\delta_1+\delta_2<2\tau_0. \tag{A.17}$$

When the delays in both modes are equivalent, $\delta_1=\delta_2=\delta$, we find the condition for interference is

$$0\le\delta\le\tau_0. \tag{A.18}$$

Using the identities

$$\sin\theta x=\frac{1}{2i}\left(e^{i\theta x}-e^{-i\theta x}\right) \tag{A.19}$$

and

$$\int_0^\infty dx\, e^{-p^2x^2}\frac{\sin ax}{x}=\frac{\pi}{2}\operatorname{erf}\left(\frac{a}{2p}\right) \tag{A.20}$$

where $\operatorname{erf}(x)$ is the error function,

$$\operatorname{erf}(x) = \frac{\sqrt{\pi}}{2}\int_0^x e^{-t^2}\,dt\,, \tag{A.21}$$

we find

$$A = \frac{\pi^2}{2\left(b^2 - a^2\right)}\left[\operatorname{erf}\left(\frac{\left(\Delta + \left(2 - \left|2 + \Sigma'\right|\right)\alpha\right)}{2}\sigma\right) - \operatorname{erf}\left(\frac{\left(\Delta - \left(2 - \left|2 + \Sigma'\right|\right)\alpha\right)}{2}\sigma\right)\right]. \tag{A.22}$$

Rewritten in terms of the two delays, this yields

$$\begin{aligned} A = \frac{\pi^2}{2\left(b^2 - a^2\right)}\Bigg\{&\left(\operatorname{erf}\left(\frac{\sigma\left(\delta_1\tau_b + \delta_2\tau_a\right)}{2\tau_0}\right) + \operatorname{erf}\left(\frac{\sigma\left(\delta_1\tau_a + \delta_2\tau_b\right)}{2\tau_0}\right)\right)\Pi\left[\delta_1 + \delta_2; 0, \tau_0\right] \\ &+\left(\operatorname{erf}\left(\frac{\sigma\left(\left(\tau_0 - \delta_1\right)\tau_b + \left(\tau_0 - \delta_2\right)\tau_a\right)}{2\tau_0}\right)\right. \\ &\left.+ \operatorname{erf}\left(\frac{\sigma\left(\left(\tau_0 - \delta_1\right)\tau_a + \left(\tau_0 - \delta_2\right)\tau_b\right)}{2\tau_0}\right)\right)\Pi\left[\delta_1 + \delta_2; \tau_0, 2\tau_0\right]\Bigg\}. \end{aligned} \tag{A.23}$$

For the case $\delta_1 = \delta_2 = \delta$ this results reduces to

$$A = \frac{\pi^2}{\left(b^2 - a^2\right)}\left\{\operatorname{erf}\left(\frac{\sigma\left(\tau_a + \tau_b\right)\delta}{2\tau_0}\right)\Pi\left(\delta; 0, \frac{\tau_0}{2}\right) + \operatorname{erf}\left(\frac{\sigma\left(\tau_a + \tau_b\right)\left(\tau_0 - \delta\right)}{2\tau_0}\right)\Pi\left(\delta; \frac{\tau_0}{2}, \tau_0\right)\right\}. \tag{A.24}$$